J|A|C|S
ARTICLES
Published on Web 07/04/2006

Determination of μ-Oxo Exchange Rates in Di-μ-Oxo Dimanganese Complexes by Electrospray Ionization Mass Spectrometry

Ranitendranath Tagore, Hongyu Chen, Robert H. Crabtree,* and Gary W. Brudvig*

Contribution from the Department of Chemistry, Yale University, P.O. Box 208107, New Haven, Connecticut 06520-8107

Received February 25, 2006; E-mail: gary.brudvig@yale.edu; robert.crabtree@yale.edu

Abstract: A time-resolved mass spectrometric technique has been used for the determination of rates of exchange of μ-O atoms with water for the complexes $[(\text{mes-terpy})_2\text{Mn}_2^{\text{III/IV}}(\mu\text{-O})_2(\text{H}_2\text{O})_2](\text{NO}_3)_3$ (**1**, mes-terpy = 4′-mesityl-2,2′:6′,2″-terpyridine), $[(\text{bpy})_4\text{Mn}_2^{\text{III/IV}}(\mu\text{-O})_2](\text{ClO}_4)_3$ (**2**, bpy = 2,2′-bipyridine), $[(\text{phen})_4\text{Mn}_2^{\text{III/IV}}(\mu\text{-O})_2](\text{ClO}_4)_3$ (**3**, phen = 1,10-phenanthroline), $[(\text{bpea})_2\text{Mn}_2^{\text{III/IV}}(\mu\text{-O})_2(\mu\text{-OAc})](\text{ClO}_4)_2$ (**4**, bpea = bis(2-pyridyl)ethylamine), $[(\text{bpea})_2\text{Mn}_2^{\text{IV/IV}}(\mu\text{-O})_2(\mu\text{-OAc})](\text{ClO}_4)_3$ (**4$^{\text{ox}}$**), $[(\text{terpy})_4\text{Mn}_4^{\text{IV/IV/IV/IV}}(\mu\text{-O})_5(\text{H}_2\text{O})_2](\text{ClO}_4)_6$ (**5**, terpy = 2,2′:6′,2″-terpyridine), and $[(\text{tacn})_4\text{Mn}_4^{\text{IV/IV/IV/IV}}(\mu\text{-O})_6]\text{Br}_{3.5}(\text{OH})_{0.5}\cdot 6\text{H}_2\text{O}$ (**6**, tacn = 1,4,7-triazacyclononane). The rate of exchange of μ-OAc bridges with free acetate in solution has been measured for complexes **4** and **4$^{\text{ox}}$**. These are the first measurements of rates of ligand exchange on biologically relevant high-valent Mn complexes. The data analysis method developed here is of general utility in the quantitation of isotope exchange processes by mass spectrometry. We find that the presence of labile coordination sites on Mn increases μ-O exchange rates, and that all-Mn^{IV} states are more inert toward exchange than mixed Mn^{III}–Mn^{IV} states. The rates of μ-O exchange obtained in this work for a di-μ-oxo $\text{Mn}_2^{\text{III/IV}}$ dimer with labile coordination sites are compared with the oxygen isotope incorporation rates from substrate water to evolved dioxygen measured in different S states of the oxygen evolving complex (OEC) of photosystem II (PSII). On the basis of this comparison, we propose that both substrate waters are not bound as μ-O bridges between Mn atoms in the S_2 and S_3 states of the OEC.

Introduction

Photosynthetic O_2 evolution, catalyzed by the O_2-evolving complex (OEC) of photosystem II (PSII), converts two H_2O molecules into O_2. Recent progress in the X-ray crystallography of PSII[1−5] has enabled the modeling of the OEC as a cuboidal Mn_3CaO_4 structure connected to a fourth Mn via a μ-O bridge.[3] The mechanisms proposed in the literature involve the binding of substrate H_2O molecules as ligands to the Ca and/or Mn ions in the OEC. The substrate waters are proposed to undergo oxidation either when bound as terminal ligands[6−11] or via incorporation into the μ-O bridges between Mn ions.[11−16]

Information on the waters bound in the OEC has been obtained from measurements of the rates of isotope exchange between substrate waters and bulk $H_2{}^{18}O$.[17−21] Isotope exchange in the OEC may involve complex pathways, and only the evolved O_2 can be analyzed, precluding the direct observation of exchange kinetics of specific ligands. Investigation of ligand exchange in model complexes will, therefore, help to provide a basis for interpretation of the biological experiments, and may reveal the nature of H_2O-binding sites in the OEC.

^{17}O NMR has been used to measure the rate of H_2O exchange in $[\text{Mn}(\text{H}_2\text{O})_6]^{2+}$ ($k \approx 2 \times 10^7\ \text{s}^{-1}$),[22] but no ligand exchange rates have yet been determined on biologically relevant high-valent oxomanganese complexes. Exchange of the μ-O bridges has been demonstrated in a di-μ-oxo $\text{Mn}_2^{\text{III/IV}}$ dimer[23] and a

(1) Zouni, A.; Witt, H.-T.; Kern, J.; Fromme, P.; Krauss, N.; Saenger, W.; Orth, P. *Nature (London)* **2001**, *409*, 739−743.
(2) Kamiya, N.; Shen, J.-R. *Proc. Natl. Acad. Sci. U.S.A.* **2003**, *100*, 98−103.
(3) Ferreira, K. N.; Iverson, T. M.; Maghlaoui, K.; Barber, J.; Iwata, S. *Science* **2004**, *303*, 1831−1838.
(4) Biesiadka, J.; Loll, B.; Kern, J.; Irrgang, K.-D.; Zouni, A. *Phys. Chem. Chem. Phys.* **2004**, *6*, 4733−4736.
(5) Loll, B.; Kern, J.; Saenger, W.; Zouni, A.; Biesiadka, J. *Nature (London)* **2005**, *438*, 1040−1044.
(6) Hoganson, C. W.; Babcock, G. T. *Science* **1997**, *277*, 1953−1956.
(7) Haumann, M.; Junge, W. *Biochim. Biophys. Acta* **1999**, *1411*, 86−91.
(8) Schlodder, E.; Witt, H. T. *J. Biol. Chem.* **1999**, *274*, 30387−30392.
(9) Pecoraro, V. L., Hsieh, W.-Y. *Manganese and Its Role in Biological Processes*; Sigel, H., Sigel, A., Eds.; Metal Ions in Biological Systems, Vol. 37; Marcel Dekker: New York, 2000; pp 429−504.
(10) McEvoy, J. P.; Brudvig, G. W. *Phys. Chem. Chem. Phys.* **2004**, *6*, 4754−4763.
(11) Messinger, J. *Phys. Chem. Chem. Phys.* **2004**, *6*, 4764−4771.
(12) Brudvig, G. W.; Crabtree, R. H. *Proc. Natl. Acad. Sci. U.S.A.* **1986**, *83*, 4586−4588.
(13) Pecoraro, V. L.; Baldwin, M. J.; Gelasco, A. *Chem. Rev.* **1994**, *94*, 807−826.
(14) Yachandra, V. K.; Sauer, K.; Klein, M. P. *Chem. Rev.* **1996**, *96*, 2927−2950.
(15) Nugent, J. H. A.; Rich, A. M.; Evans, M. C. W. *Biochim. Biophys. Acta* **2001**, *1503*, 138−146.
(16) Robblee, J. H.; Cinco, R. M.; Yachandra, V. K. *Biochim. Biophys. Acta* **2001**, *1503*, 7−23.
(17) Messinger, J.; Badger, M.; Wydrzynski, T. *Proc. Natl. Acad. Sci. U.S.A.* **1995**, *92*, 3209−3213.
(18) Hillier, W.; Messinger, J.; Wydrzynski, T. *Biochemistry* **1998**, *37*, 16908−16914.
(19) Hillier, W.; Wydrzynski, T. *Biochemistry* **2000**, *39*, 4399−4405.
(20) Hendry, G.; Wydrzynski, T. *Biochemistry* **2002**, *41*, 13328−13334.
(21) Hendry, G.; Wydrzynski, T. *Biochemistry* **2003**, *42*, 6209−6217.
(22) Ducommun, Y.; Newman, K. E.; Merbach, A. E. *Inorg. Chem.* **1980**, *19*, 3696−3703.

mono-μ-oxo $Mn_2^{III/III}$ dimer,[24] based on IR and Raman spectral changes upon the addition of $H_2{}^{18}O$. These techniques, however, have not been used for kinetic analysis, and rates were not reported in either case.

We report here the use of a time-resolved mass spectrometric technique for the determination of μ-O exchange rates in di-μ-oxo dimanganese complexes. The complexes studied are $[(\text{mes-terpy})_2Mn_2^{III/IV}(\mu\text{-O})_2(H_2O)_2](NO_3)_3$ (**1**, mes-terpy = 4′-mesityl-2,2′:6′,2″-terpyridine), $[(\text{bpy})_4Mn_2^{III/IV}(\mu\text{-O})_2](ClO_4)_3$ (**2**, bpy = 2,2′-bipyridine), $[(\text{phen})_4Mn_2^{III/IV}(\mu\text{-O})_2](ClO_4)_3$ (**3**, phen = 1,10-phenanthroline), $[(\text{bpea})_2Mn_2^{III/IV}(\mu\text{-O})_2(\mu\text{-OAc})](ClO_4)_2$ (**4**, bpea = bis(2-pyridyl)ethylamine), $[(\text{bpea})_2Mn_2^{IV/IV}(\mu\text{-O})_2(\mu\text{-OAc})](ClO_4)_3$ (**4^{ox}**), $[(\text{terpy})_4Mn_4^{IV/IV/IV/IV}(\mu\text{-O})_5(H_2O)_2](ClO_4)_6$ (**5**, terpy = 2,2′:6′,2″-terpyridine), and $[(\text{tacn})_4Mn_4^{IV/IV/IV/IV}(\mu\text{-O})_6]Br_{3.5}(OH)_{0.5}\cdot 6H_2O$ (**6**, tacn = 1,4,7-triazacyclononane). In an earlier report, Cooper et al. found that μ-O exchange occurred only at elevated temperatures for **2** and **3** in aqueous solution.[23] In contrast, we find μ-O exchange at room temperature with trace amounts of water in acetonitrile. We have also measured the rate of the exchange of μ-OAc bridges with free acetate in solution for complexes **4** and **4^{ox}**. The μ-OAc exchange process is of potential relevance to the process of acetate inhibition of PSII.[25−29]

The technique described here allows the ligand exchange kinetics of the **4** and **4^{ox}** valence states to be followed in the same solution and potentially has wide applications in the study of isotope exchange reactions. The data analysis method using the total intensity of an isotope pattern for normalization allows the quantitation of fractions of species in exchange, thus yielding the kinetics of the exchange process (see Data Analysis section). The normalization also corrects for the intensity fluctuations inherent in ESI-MS experiments and affords good signal/noise ratio.

Experimental Section

Materials. Reagents were used as received. Acetonitrile (HPLC grade) was purchased from Fisher Scientific. Glacial acetic acid was obtained from J.T. Baker. $H_2{}^{18}O$ (95 atom % ^{18}O) was purchased from Icon Stable Isotopes. CD_3COOD (99.5 atom % D) was purchased from Sigma Aldrich. Compounds **1**−**6** were synthesized according to literature procedures.[23,30−35]

ESI-MS. Spectra were collected on a Waters/Micromass ZQ 4000 mass spectrometer and processed with the Masslynx (V 4.0) software. In a typical run, ∼300−800 μL of a ∼200−600 μM MeCN solution of manganese complex was mixed with ∼3−6 μL of $H_2{}^{18}O$. The resultant solution was monitored by two different modes of data acquisition, according to the speed of the exchange process.

(a) Continuum. When the exchange process was relatively fast (occurring in ∼30 min or less), the data acquisition software was started in the continuum mode at the time of mixing reactants. In this mode, the software continues recording spectra at specified time intervals (typically 2.5 s in our experiments) until a specified end time, with the time of start of data acquisition being set as zero time. To meet the requirements of good signal-to-noise ratio and fast data collection, only a narrow region containing the peak of interest was scanned. A relatively large volume of reaction solution (∼500 μL) was loaded into the syringe that fed into the mass spectrometer, and the syringe continued to run (∼20 μL/min) until the end of the experiment. Even though the time delay between successive spectra was only of the order of a second, reactions that are complete within ∼100 s were not time resolved by this method due to the time required for loading the sample syringe and for the sample to go through the lines into the detector.

(b) Multiple Channel Averaging (MCA). When the exchange process was relatively slow, a stopwatch was started at the time of mixing reactants. A small volume (∼30 μL) of reaction solution was then loaded into a syringe. When the sample reached the detector (as shown by the appearance of peaks of constant and high intensity), data collection was started in the MCA mode, and the time on the stopwatch was noted. In the MCA mode, data were collected over a specified time period (typically 12 s in our experiments), and all the scans collected during this period were averaged into a single spectrum. Since the data collection time is small with respect to the total reaction time, we can take the averaged spectrum to be representative of the true spectrum at the mid-point time in the acquisition (6 s after start of acquisition for a 12-s scan). This process was repeated at intervals of 5−30 min to obtain the time course of exchange.

Data Analysis

Assignment of ESI-MS Peaks. Molecular formulas of species were put into the isotope distribution calculator program at http://www2.sisweb.com/mstools/isotope.htm to obtain calculated *m*/*z* values and isotope ratios. Initial assignments of experimental spectra were based upon the *m*/*z* values and isotope ratios. For simulation of experimental spectra, molecular formulas were put into the Masslynx V 4.0 program. The Gaussian peak widths in the theoretical isotope distribution output were adjusted to match the observed experimental isotope distribution while maintaining the calculated relative peak areas at different *m*/*z* values in the theoretical isotope pattern.

Analysis of Mass Spectral Intensity Data. The isotope pattern obtained in the mass spectrum due to a given chemical species is altered upon isotope exchange. In the present work, heavier isotopes are incorporated in place of lighter ones, so that the peak at the lowest mass in the isotope pattern decreases in intensity, and the isotope pattern "spreads" to higher masses. The overall isotope pattern at any time during exchange is, therefore, a superposition of the isotope patterns due to unexchanged and exchanged species. The signal intensities due to unexchanged and exchanged species are deconvoluted from each spectrum and normalized against total intensity to obtain concentrations of unexchanged and exchanged species, as explained below.

(a) $^{16}O-{}^{18}O$ Exchange. The compounds used in the present study contain several types of oxygen: μ-O, μ-OAc, NO_3^-, ClO_4^-. In compounds **1**−**4^{ox}** only the two μ-O oxygens undergo exchange with the oxygens of added $H_2{}^{18}O$, while we did not observe any exchange in compounds **5** and **6**. We, therefore, derive below the formulas for obtaining the extent of exchange

(23) Cooper, S. R.; Calvin, M. *J. Am. Chem. Soc.* **1977**, *99*, 6623−6630.
(24) Sheats, J. E.; Czernuszewicz, R. S.; Dismukes, G. C.; Rheingold, A. L.; Petrouleas, V.; Stubbe, J.; Armstrong, W. H.; Beer, R. H.; Lippard, S. J. *J. Am. Chem. Soc.* **1987**, *109*, 1435−1444.
(25) Kelley, P. M.; Izawa, S. *Biochim. Biophys. Acta* **1978**, *502*, 198−210.
(26) Sinclair, J. *Biochim. Biophys. Acta* **1984**, *764*, 247−252.
(27) Sandusky, P. O.; Yocum, C. F. *Biochim. Biophys. Acta* **1986**, *849*, 85−93.
(28) MacLachlan, D. J.; Nugent, J. H. A.; Warden, J. T.; Evans, M. C. W. *Biochim. Biophys. Acta* **1994**, *1188*, 325−334.
(29) Kuehne, H.; Szalai, V. A.; Brudvig, G. W. *Biochemistry* **1999**, *38*, 6604−6613.
(30) Chen, H.; Tagore, R.; Das, S.; Incarvito, C. D.; Faller, J. W.; Crabtree, R. H.; Brudvig, G. W. *Inorg. Chem.* **2005**, *44*, 7661−7670.
(31) Manchanda, R.; Brudvig, G. W.; de Gala, S.; Crabtree, R. H. *Inorg. Chem.* **1994**, *33*, 5157−5160.
(32) Pal, S.; Olmstead, M. M.; Armstrong, W. H. *Inorg. Chem.* **1995**, *34*, 4708−4715.
(33) Pal, S.; Chan, M. K.; Armstrong, W. H. *J. Am. Chem. Soc.* **1992**, *114*, 6398−6406.
(34) Chen, H.; Faller, J. W.; Crabtree, R. H.; Brudvig, G. W. *J. Am. Chem. Soc.* **2004**, *126*, 7345−7349.
(35) Wieghardt, K.; Bossek, U.; Gebert, W. *Angew. Chem., Int. Ed. Engl.* **1983**, *22*, 328−329.

for compounds with two exchangeable oxygens. However, the calculations can be readily extended to the case of a higher number of exchangeable oxygens.

Let the total number of molecules of the observed species be N_T, with a natural isotope distribution between masses M and $M + n$. Upon exchange of one or both μ-O oxygens, molecules change mass by two or four, respectively. Therefore, molecules originally with mass M, will have mass M, $M + 2$, or $M + 4$ after addition of $H_2{}^{18}O$. There will always be some unexchanged molecules due to the presence of significant concentrations of background $H_2{}^{16}O$. The total number of molecules, N_T, is now distributed between masses M to $M + n + 4$. Also, the number of molecules N with masses M, $M + 2$, $M + 4$, ..., and the number of molecules N' with masses $M + 1$, $M + 3$, $M + 5$, ... remain constant throughout the exchange, as molecules change mass by 0, 2, or 4 units. Therefore, either of N_T, N, or N' can be used as a normalization factor. It is convenient to use N or N' since a smaller number of peaks have to be tracked.

At any time during exchange, let U, S, and D be the fractions of molecules within the set of molecules N with 0, 1, or 2 ^{18}O atoms at the exchangeable sites, respectively. The resultant mass distribution is a combination of three identical overlapping mass distributions scaled by U, S, and D, and starting at masses M, $M + 2$, and $M + 4$, respectively. The basis distribution making up the resultant distribution is obtained from the isotope distribution calculator program by putting in the formula of the molecule under consideration, minus the number of exchangeable oxygen atoms (two in the present case). Let the fraction of molecules at mass M in the calculated distribution be f_m. Denoting the intensity due to N molecules by I, and noting that signal intensity at mass M (I_M) is proportional to the number of molecules with mass M, we get

$$I_M/I = (UNf_m)/N = Uf_m \tag{1a}$$

$$I_{M+2}/I = (SNf_m + UNf_{m+2})/N = Sf_m + Uf_{m+2} \tag{1b}$$

(the second term is due to overlap with the distribution starting at M).

$$I_{M+4}/I = (DNf_m + SNf_{m+2} + UNf_{m+4})/N = Df_m + Sf_{m+2} + Uf_{m+4} \tag{1c}$$

(second and third terms due to overlap with distributions starting at $M + 2$, and M, respectively). Note that we have equated mass to the ratio, mass/charge, because we are always looking at monopositive ions in this study.

From eq 1a, we get

$$U = (1/f_mI)(I_M) \tag{2}$$

Substituting for U from eq 2 into eq 1b,

$$S = (1/f_mI)(I_{M+2} - (f_{m+2}/f_m)I_M) \tag{3}$$

Finally, substituting for U and S from eqs 2 and 3 into eq 1c,

$$D = (1/f_mI)(I_{M+4} - (f_{m+2}/f_m)I_{M+2} - (f_{m+4}/f_m - f^2{}_{M+2}/f^2{}_M)I_M) \tag{4}$$

This gives us the fractions of molecules with zero, one, or two ^{18}O atoms at the exchangeable sites. In other words, we have the fractions of unexchanged (U), singly exchanged (S), and doubly exchanged (D) molecules in terms of measured intensities and calculated isotope distribution patterns. In the final plots of the time course of species in exchange, fractions were converted to percentages.

(b) CH_3COO^-/CD_3COO^- Exchange. We observed the exchange of one CH_3COO^- by one CD_3COO^-. Thus, exchange causes the incorporation of zero, or three D atoms. Let the fractions of unexchanged and exchanged molecules be U and E, respectively.

As before, let the natural isotope distribution of the species under observation be between masses M and $M + n$, and the number of molecules N with masses M, $M + 3$, $M + 6$, ... is constant over the course of exchange, and is a constant fraction of the total number of molecules N_T. With considerations similar to those noted for $^{16}O-{}^{18}O$ exchange, we get

$$I_M/I = f_mU \tag{5a}$$

$$I_{M+3}/I = f_{m+3}U + f_mE \tag{5b}$$

which rearrange to

$$U = (1/f_m)(I_M/I) \tag{6}$$

$$E = (1/f_mI)(I_{M+3} - (f_{m+3}/f_m)I_M) \tag{7}$$

General Considerations

Quantitation of Species by ESI-MS. Gas-phase mass spectrometry has commonly been used for the quantitation of gaseous species. However, there are two principal difficulties in attempting quantitative mass spectrometry of solutions. First, the "response factor" of a mass spectrometer, or the relationship between signal intensity and concentration of species, is different for different chemical species. Second, the response factor varies from one scan to another, so that the same concentration of a given species will produce different signal intensities in different scans. However, the first problem does not apply to this work, because the different species that we are trying to quantitate are isotopes of each other and, therefore, should have equivalent response factors. The fact that the experimental isotope patterns, in the absence of exchange, match with calculated isotope patterns shows that mass spectrometers do have very similar response factors for isotopes of a given chemical species. The second problem is solved by our data analysis method of dividing the intensity at a given m/z value (I_M) by the total intensity of the isotope pattern (I). This cancels the effects of the signal fluctuations from one scan to another inherent in the ESI-MS instrument and yields the relative proportions of exchange states. These can then be converted to actual concentrations by normalizing to the total concentration of the complex, which is unchanged during the isotope exchange process.

Quantitation of species by ESI-MS has been applied to chemical reactions by calibrating intensities against nonreacting internal standards[36] or known concentrations of reacting species.[37,38] Using the signal intensity from a known concentration

(36) Konermann, L.; Collings, B. A.; Douglas, D. J. *Biochemistry* **1997**, *36*, 5554−5559.
(37) Attwood, P. V.; Geeves, M. A. *Anal. Biochem.* **2004**, *334*, 382−389.
(38) Li, Z.; Sau, A. K.; Furdui, C. M.; Anderson, K. S. *Anal. Biochem.* **2005**, *343*, 35−47.

of reacting species obtained from a different scan as a calibration factor, does not correct for intensity fluctuations of the ESI-MS instrument from one scan to another (although this effect may be small in general), and the calibration varies with instrumental conditions such as flow rate.[37] The use of nonreacting internal standards, on the other hand, may be limited by the availability of suitable standards. Moreover, the Mn complexes measured in this study give weak ESI-MS signals. Therefore, real-time data acquisition requires fast data collection over a narrow *m*/*z* range, and thus the signal from any internal standard used must necessarily be very close to the signal of interest, imposing another limitation on the use of internal standards. Thus, for monitoring isotope exchange reactions, our method of signal normalization affords a convenient and rigorous method of quantitation of reaction progress.

Time Resolution of ESI-MS Experiments. Real-time monitoring of ESI-MS spectra with a continuous sample introduction setup has been reported by Lee et al.[39] and Sam et al.[40,41] The time resolution of these early experiments has been greatly improved by later workers through the use of low-volume mixing tees and capillary tubes (of well-defined length and diameter) interfaced to the ionization source of the mass spectrometer. Such setups avoid real-time data acquisition and can achieve time resolutions of about half a second,[37] and even down to a few milliseconds,[38,42] without the requirement of fast data acquisition capability. In the present study, however, we have used an unmodified commercially available ESI-MS setup, where the time resolution is limited by the time taken to transfer the sample to the detector after mixing of reactants (~1.5 min).

Effect of the ESI Process on Kinetic Data. The high temperatures experienced during the electrospray process are likely to speed up the exchange reactions, but this effect should be equivalent for each measurement, irrespective of the time at which the sample is subjected to the electrospray process. The change in the spectrum recorded from one time point to the next, therefore, represents the change that occurred in that same time interval at room temperature (which is what the sample experiences before ionization). Heating does, however, cause a change in the amount of exchange by a constant proportion, and the resultant offset can be estimated by fitting the experimental time-dependent curves to an appropriate equation and extrapolating to zero time. For example, the curves obtained for U in $^{16}O-^{18}O$ exchange experiments fit to a single-exponential decay. We expect that at the time of $H_2{}^{18}O$ addition (zero time), there will be 100% U, and no S or D. However, the curve for U extrapolates to less than 100% at zero time, and 100% is reached upon extrapolation to a negative value for time. This implies that there is more reaction than predicted by the exponential fit, which assumes a constant observed rate constant (k_{obs}). It is likely, therefore, that the reaction proceeds more rapidly during the ionization process, giving rise to an "excess" reaction. In other words, the reaction would have taken longer in absence of the accelerated reaction during ionization. This time difference is given by the value of time at which the exponential extrapolates back to 100% and was typically about 70 s for the continuum mode experiments.

Ligand Exchange Rates by NMR, Infrared (IR), and Raman Spectroscopies. NMR spectroscopy has been the technique of choice for obtaining solvent exchange kinetics due to the wide range of rates accessible to study.[43] IR and Raman spectroscopies have been used to monitor isotope exchange processes and could be used to study exchange between labeled and unlabeled solvent. However, in the present study, ESI-MS has significant advantages over these techniques.

NMR generally requires significantly higher concentrations of sample as compared to ESI-MS. This problem is magnified in the case of paramagnetic metal complexes (such as the present ones) which give very broad NMR signals. The minute-scale exchange processes being studied, therefore, are more conveniently studied by ESI-MS.

Examples of the use of solution IR spectroscopy are not very common,[44] and generally require extremely high sample concentrations. Solid-phase IR is disadvantageous in requiring quenching of the reaction and drying of the sample.[23,45] Raman spectroscopy is preferred over IR for monitoring exchange rates because solution spectra can be acquired, and setups have been built to achieve time resolutions of ~1 min.[46] However, it still requires high sample concentrations as compared to those for ESI-MS.

Results and Discussion

ESI-Mass Spectra. The use of nonaqueous solvents is advantageous for isotope-labeling experiments with labeled water. This is because even a small amount of labeled water achieves a high labeling ratio, in contrast to aqueous media, where there are very large amounts of unlabeled water present. Acetonitrile-soluble manganese complexes were, therefore, used in the present study. The structures of complexes used are shown in Figure 1. The spectra of complexes **1**−**6** in acetonitrile are quite complex due to fragmentation during the ESI process, and the extent of fragmentation varies considerably from one complex to another. The solutions themselves, however, are stable over the time course of the experiments, as verified by EPR and UV−visible spectra. Thus, all fragments observed by ESI-MS originate from the pure compound, and the label incorporation in all fragments should reflect the label incorporation in the parent compound in solution. The spectrum of **1** is shown in Figure 2.

The peaks visible in the positive ion ESI-MS can be attributed to pairing of anions available in solution with cationic species generated from the manganese complexes by ligand coordination and decoordination, by the fragmentation shown in Scheme 1, and by the aggregation of fragments. Thus, in the spectrum of **1**, we observe the free ligand mes-terpy (peak 1), Mn^{II} species (peaks 2, 4, 5), and Mn^{V} species (mes-terpy)$Mn^{V}O_2$ (peak 3) formed by the above-mentioned fragmentation, and the native dimeric species with water ligands lost[30] (peaks 6, 7). The assignment of the Mn^{V} species was confirmed by addition of $H_2{}^{18}O$, which showed the presence of two exchangeable oxygens, and by exchange with several other substituted

(39) Lee, E. D.; Muck, W.; Henion, J. D.; Covey, T. R. *J. Am. Chem. Soc.* **1989**, *111*, 4600−4604.
(40) Sam, J. W.; Tang, X.-J.; Peisach, J. *J. Am. Chem. Soc.* **1994**, *116*, 5250−5256.
(41) Sam, J. W.; Tang, X.-J.; Magliozzo, R. S.; Peisach, J. *J. Am. Chem. Soc.* **1995**, *117*, 1012−1018.
(42) Pan, J.; Rintala-Dempsey, A. C.; Li, Y.; Shaw, G. S.; Konermann, L. *Biochemistry* **2006**, *45*, 3005−3013.
(43) Helm, L.; Merbach, A. E. *Chem. Rev.* **2005**, *105*, 1923−1960.
(44) Larson, D. L.; McLaughlin, J., Jr. *J. Am. Chem. Soc.* **1955**, *77*, 1359−1360.
(45) Murmann, R. K. *Inorg. Chem.* **1980**, *19*, 1765−1770.
(46) Li, T.; Johnson, J. E.; Thomas, G. J., Jr. *Biophys. J.* **1993**, *65*, 1963−1972.

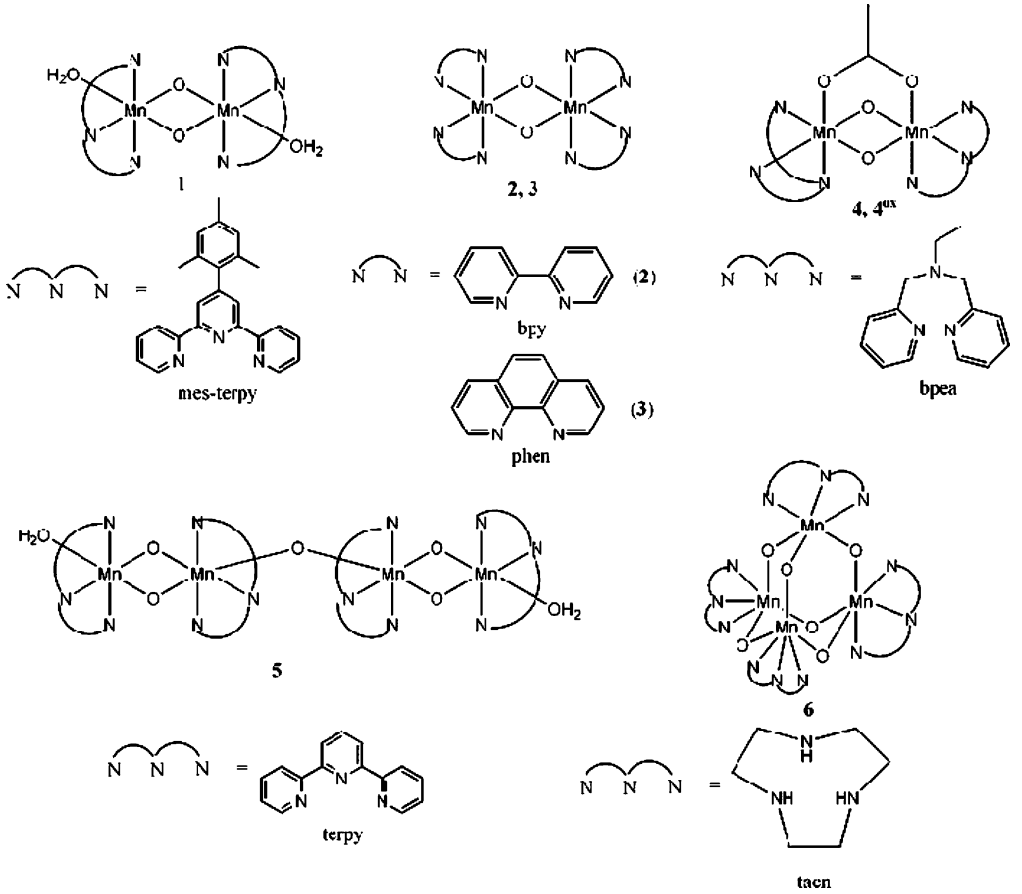

Figure 1. Structure of complexes used. Abbreviations used in the text for ligands are indicated.

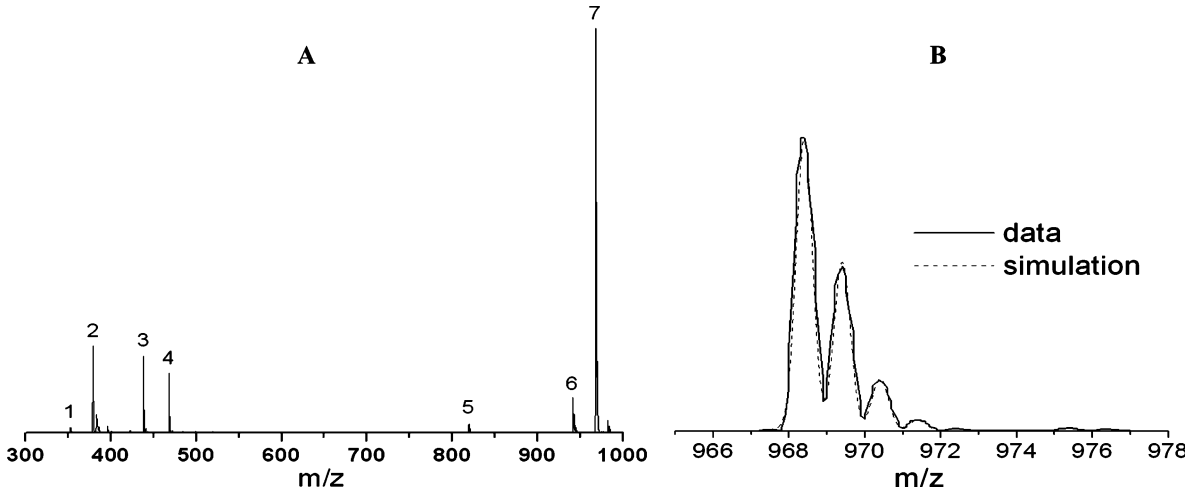

Figure 2. Positive ion ESI mass spectrum of **1** in acetonitrile. (Panel A) Full spectrum. The *m*/*z* values and assignments of labeled peaks are as follows: (1) 352, mes-terpyH$^+$; (2) 378.5, [(mes-terpy)$_2$Mn^{II}]$^{2+}$; (3) 438, [(mes-terpy)Mn^{V}O$_2$]$^+$; (4) 468, [(mes-terpy)Mn^{II}(NO$_3$)]$^+$; (5) 819, [(mes-terpy)$_2$Mn^{II}(NO$_3$)]$^+$; (6) 941, [(mes-terpy)$_2$Mn$_2^{III/IV}$O$_2$(NO$_3$)Cl]$^+$; (7) 968, [(mes-terpy)$_2$Mn$_2^{III/IV}$O$_2$(NO$_3$)$_2$]$^+$. (Panel B) Expanded view of peak 7, along with the calculated isotope pattern for the assigned species (dotted line). The shift in isotope pattern of peak 7 upon the addition of labeled water was followed to obtain μ-O exchange kinetics for **1**.

Scheme 1. Proposed Fragmentation of Oxomanganese Core under ESI-MS Conditions

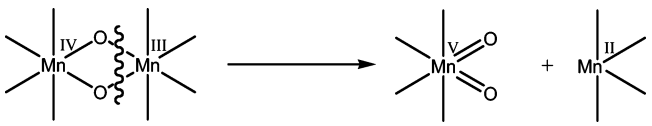

terpyridine ligands, which confirmed the presence of one terpyridine ligand. Na^+ and Cl^- are found to be ubiquitous in the mass spectrometer even after careful rinsing of sample channels, and peak 6 is due to ion-pairing with such adventitious Cl^-. Because peaks 6 and 7 are assigned to species containing μ-O bridges, the isotope incorporation in either of these peaks will reflect the isotope incorporation in the μ-O bridges of **1** in solution. The more intense peak 7 was followed in this study. The satellite peaks at $m/z = 969-973$ accompanying the most intense peak at $m/z = 968$ are due to the natural abundance of heavy isotopes of C, H, N, and O. This needs to be accounted for in calculating the fractions of U, S, and D, because there is

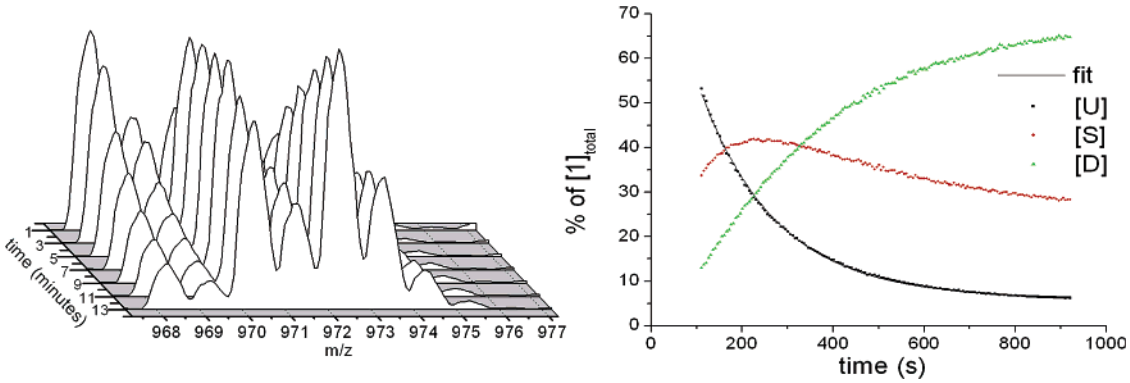

Figure 3. μ-O exchange of **1** by ESI-MS. (Left panel) Changes in the isotope pattern of peak 7, assigned as $[(\text{mes-terpy})_2\text{Mn}_2^{\text{III/IV}}\text{O}_2(\text{NO}_3)_2]^+$, in the ESI mass spectrum of **1** in acetonitrile upon the addition of $H_2{}^{18}O$. (Right panel) Percentages (of total **1**) of unexchanged (U), singly exchanged (S), and doubly exchanged (D) complex extracted, as explained in main text, from peak intensities. The trace for U contains an exponential fit, which is not clearly visible due to the large number of data points and the closeness of the fit. The fit yields the observed rate constant for the exchange, listed in Table 1.

Table 1. Observed Rate Constants Obtained at 20 °C for μ-O and μ-OAc Exchange Processes

reactants[a]	ligand exchanged	k_{obs} (s^{-1}), $t_{1/2}$ (s)	oxidation state of Mn
1 + $H_2{}^{18}O$	μ-O	$(2.5 \pm 0.2) \times 10^{-3}$, 280 ± 20	$Mn_2^{III/IV}$
2 + $H_2{}^{18}O$	μ-O	$(5.4 \pm 0.2) \times 10^{-4}$, 1280 ± 50	$Mn_2^{III/IV}$
3 + $H_2{}^{18}O$	μ-O	$(6 \pm 1) \times 10^{-4}$, 1200 ± 200	$Mn_2^{III/IV}$
4 + $H_2{}^{18}O$	μ-O	$(4.5 \pm 0.2) \times 10^{-4}$, 1540 ± 70	$Mn_2^{III/IV}$
4^{ox} + $H_2{}^{18}O$	(a) μ-O in **4**	(a) $(3.2 \pm 0.3) \times 10^{-4}$, 2200 ± 200[b]	$Mn_2^{III/IV}$ (present in a solution of **4**^{ox})
	(b) μ-O in **4**^{ox}	(b) $(5.0 \pm 0.3) \times 10^{-5}$, 13900 ± 800[b]	$Mn_2^{IV/IV}$
4 + CD_3COOD	μ-OAc	$\geq 5.5 \times 10^{-2}$, ≤ 13	$Mn_2^{III/IV}$
4^{ox} + CD_3COOD	(a) μ-OAc in **4**	(a) $\geq 5.5 \times 10^{-2}$, ≤ 13	$Mn_2^{III/IV}$ (present in a solution of **4**^{ox})
	(b) μ-OAc in **4**^{ox}	(b) $(1.6 \pm 0.1) \times 10^{-4}$, 4300 ± 300[b]	$Mn_2^{IV/IV}$
5 + $H_2{}^{18}O$	μ-O	$\leq 2 \times 10^{-7}$, $\geq 3 \times 10^6$	$Mn_4^{IV/IV/IV/IV}$
6 + $H_2{}^{18}O$	μ-O	$\leq 1 \times 10^{-8}$, $\geq 6 \times 10^7$	$Mn_4^{IV/IV/IV/IV}$

[a] [Mn-complexes] = 600 μM, [$H_2{}^{18}O$] = 260 mM, [CD_3COOD] = 550 μM. [b] Rates measured in solutions containing both **4** and **4**^{ox} represent the lower limit and upper limit, respectively, for exchange processes in **4** and **4**^{ox}, to account for the possibility of interconversion between **4** and **4**^{ox} (see text).

overlap between the parent peaks of a given isotopomer with satellite peaks from the other isotopomers. This deconvolution is achieved by the formulas developed in the Data Analysis section. Similarly, peaks assigned to native dimeric or tetrameric species containing μ-O bridges were followed for obtaining μ-O exchange kinetics of other complexes.

For **4** and **4**^{ox}, the dimeric species also contains the μ-OAc bridge, and thus yields the kinetics of μ-OAc exchange upon addition of CD_3COOD. The loss of coordinated water ligands during the ESI process, as noted above, precludes the measurement of the exchange rate of the terminal H_2O ligands of **1**. In any case, this exchange is likely to be too fast to be resolved by the present method.

Complex 1. The change with time in the isotope pattern of peak 7 upon addition of $H_2{}^{18}O$ is shown in Figure 3, left panel. In a typical run, the changes are complete within ~15 min of addition of $H_2{}^{18}O$, with the intensity of the parent peak at $m/z = 968$ dropping to ~2−5% of its original intensity. This change is too rapid to be tracked accurately by manually acquiring spectra at different times during the reaction, because it typically takes at least ~2−3 min to start the next scan after finishing the previous one. Therefore, the automated "continuum" mode of data acquisition, as described in the Experimental Section, was used, allowing spectra to be recorded every ~2−5 s. Data used in Figure 3 consist of spectra recorded at intervals of 2.5 s, and every 48th spectrum is plotted in the left panel, starting from the 24th.

To extract the kinetics of exchange, we need to follow the time course of the set of peaks at 968, 970, 972, and 974. Because molecules change mass by units of 2 upon $^{16}O-{}^{18}O$ exchange, the masses 969, 971, ... do not need to be tracked. This is explained in more detail in the Data Analysis section. Note that, even after completion of exchange, there is negligible intensity at $m/z = 976$, and so we do not need to track any further than 974. The time profile of concentrations of unexchanged (U), singly exchanged (S), and doubly exchanged (D) dimer, as extracted from these data, is shown in Figure 3, right panel. The data for U fit to a single-exponential decay of the form $A + B \exp(-k_{obs}t)$ where A, B are constants, t is time, and k_{obs} is the observed rate constant (Table 1).

To confirm that the observed changes are due to μ-O exchange, we looked for changes in peak 4 in Figure 2. This peak is assigned as $[(\text{mes-terpy})\text{Mn}^{II}(\text{NO}_3)]^+$ and shows no shift upon addition of $H_2{}^{18}O$. This confirms that there is no ^{18}O incorporation into the NO_3^- counterion. The only other oxygens available in the complex are the μ-O bridges, and must, therefore, be the sites of ^{18}O incorporation. We also note that the isotope pattern of peak 7 extends to higher mass by no more than 4 units after addition of $H_2{}^{18}O$ (as compared to the isotope pattern in the absence of $H_2{}^{18}O$), showing that there are only two oxygens that are exchangeable with water. The observation of buildup and subsequent decay of S shows that the exchange occurs sequentially, where U is converted to S, and S is subsequently converted to D.

The time of mixing the labeled water with the manganese complex is taken as zero time, but it takes additional time to load the sample and for the sample to reach the detector through

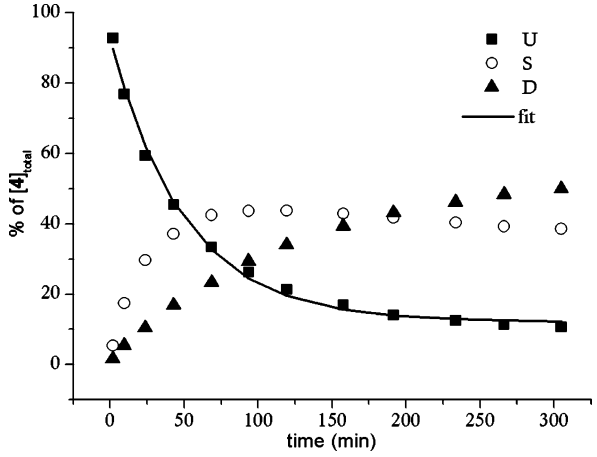

Figure 4. Percentages (of total **4**) of unexchanged (U), singly exchanged (S), and doubly exchanged (D) complex during μ-O exchange of **4** with added $H_2{}^{18}O$.

the flow lines. This is reflected by the absence of data points for the first ~100 seconds.

Complexes 4, 4^{ox}. In addition to observing μ-O exchange upon addition of labeled water, we also observed μ-OAc exchange for **4** and **4^{ox}** upon addition of CD_3COOD. As for **1**, the site of ^{18}O incorporation was confirmed to be the μ-O bridges by the shift of 4 mass units in the peaks assigned to $[(bpea)_2Mn_2^{III/IV}O_2(OAc)(ClO_4)]^+$ and $[(bpea)_2Mn_2^{IV/IV}O_2(OAc)(ClO_4)_2]^+$, and the absence of shift in the peaks assigned to $[(bpea)Mn^{II}(OAc)]^+$ and $[(bpea)_2Mn_2^{II}Cl_2(ClO_4)]^+$. The shift of 3 mass units upon addition of CD_3COOD shows that the CH_3COO^- bridge is replaced by a CD_3COO^- bridge. The rates of μ-O exchange of **4** and **4^{ox}** and for μ-OAc exchange for **4^{ox}** were found to be slow enough that the continuum mode of the mass spectrometer was not required. Instead, individual spectra were collected manually in the MCA mode (see Experimental Section) at intervals of ~5−30 min. As explained for **1**, the resultant intensity data at different *m*/*z* values allowed the percentages of species in exchange to be extracted. A plot of U, S, and D versus time for the μ-O exchange of **4** is shown in Figure 4. As for **1**, sequential conversion of U to S, and then to D, is shown by the build up and subsequent decay of S. The observed rate constant k_{obs} obtained from a single-exponential fit of the time course of U for μ-O exchange of **4**, is listed in Table 1. Exchange of the μ-OAc bridge with free acetate for **4** was found to be too fast to be resolved by our method; thus, we were only able to put a lower limit to the exchange rate.

The rates of μ-O and μ-OAc exchange for **4^{ox}** were such that the solution was not stable enough to obtain a complete time course as shown for **1** and **4** in Figures 3 and 4. Instead, only the initial linear part of the time course was recorded, and a k_{obs} value was calculated by assuming a single-exponential shape for the complete time course. The ESI-MS of **4^{ox}** shows peaks due to **4** (Figure 5, peaks 4 and 8).

The presence of **4** in the solution of **4^{ox}** was verified by EPR, which showed 16-line signals characteristic of mixed valent $Mn_2^{III/IV}$ species. Autoreduction of a $Mn_2^{IV/IV}$ complex in solution to the corresponding $Mn_2^{III/IV}$ complex has been observed by us in the case of the complex $[(terpy)_2Mn_2(\mu\text{-}O)_2(SO_4)_2]$. If electron transfer occurs to a significant extent between **4** and **4^{ox}** during the time course of the ligand exchange processes, then the observed rates of exchange for either species will not give the intrinsic rates for those species. Because a given molecule will exist in both $Mn_2^{III/IV}$ and $Mn_2^{IV/IV}$ states during the time required for ligand exchange, the observed rate of exchange will be a weighted average of the exchange rates for the two oxidation states. In the limit where interconversion between **4** and **4^{ox}** is very rapid compared to the rate of ligand exchange, the two observed rates will become equal. The fact that two very different rates are observed for **4** and **4^{ox}** for μ-O and μ-OAc exchange shows that we are not in the fast electron transfer regime. This is clearly evident from Figure 6, which shows the different extents of shift in isotope patterns of peaks assigned to $Mn_2^{III/IV}$ and $Mn_2^{IV/IV}$ species in the same solution. However, the extent to which the observed rates deviate from the intrinsic rates is still undetermined, and so we take the observed rates of ligand exchange for **4** and **4^{ox}** in the same solution to be the lower and upper limits, respectively, for the intrinsic rate.

The rate of μ-acetate exchange for **4** remains unresolvable in solutions of both **4** and **4^{ox}**, so that we put the same lower limit on both rates. However, the rates obtained for the μ-oxo exchange of **4** are slightly different in solutions of **4^{ox}** and **4**. The slightly slower rate in the solution of **4^{ox}** is consistent with the occurrence of electron transfer between **4** and **4^{ox}** as discussed above.

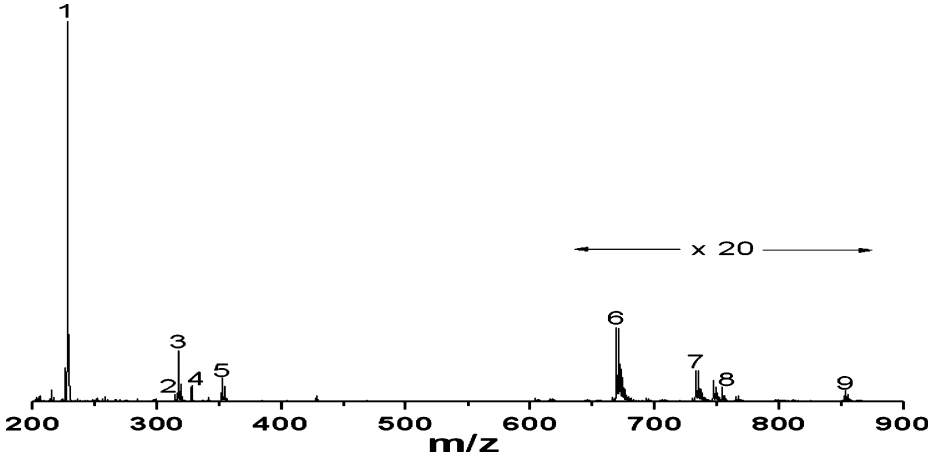

Figure 5. ESI-MS of **4^{ox}**. The *m*/*z* values and assignment of labeled peaks are as follows: (1) 228, $bpeaH^+$; (2) 314, $[(bpea)Mn^{V}O_2]^+$; (3) 317, $[(bpea)Mn_2^{II}Cl]^+$; (4) 327.5, $[(bpea)_2Mn_2^{III/IV}O_2(OAc)]^{2+}$; (5) 352, $[(bpea)Mn^{III}Cl_2]^+$; (6) 669, $[(bpea)_2Mn_2^{II}Cl_3]^+$; (7) 733, $[(bpea)_2Mn_2^{II}Cl_2(ClO_4)]^+$; (8) 754, $[(bpea)_2Mn_2^{III/IV}O_2(OAc)(ClO_4)]^+$; (9) 853, $[(bpea)_2Mn_2^{IV/IV}O_2(OAc)(ClO_4)_2]^+$.

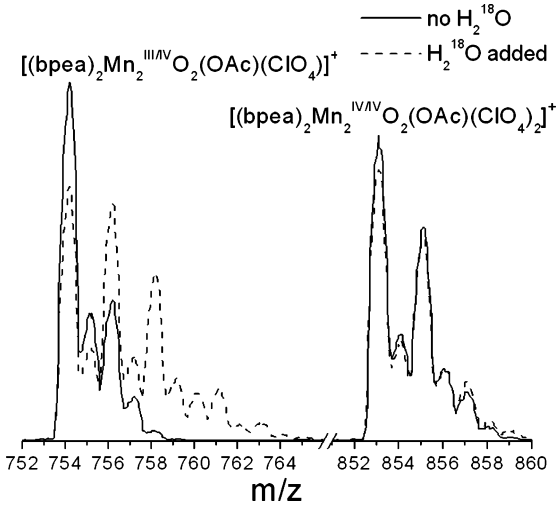

Figure 6. μ-O exchange of $Mn_2^{III/IV}$ and $Mn_2^{IV/IV}$ dimers in the same solution by ESI-MS. Peaks assigned to $[(bpea)_2Mn_2^{III/IV}(\mu\text{-}O)_2(\mu\text{-}OAc)(ClO_4)]^+$ and $[(bpea)_2Mn_2^{IV/IV}(\mu\text{-}O)_2(\mu\text{-}OAc)(ClO_4)_2]^+$ in the ESI MS of an acetonitrile solution of **4**^{ox}, before (solid line) and ~15 min after (broken line) addition of $H_2{}^{18}O$.

Complexes 2, 3. In the ESI-MS of **2** and **3**, peaks assigned to $[L_2Mn_2^{III/IV}O_2(ClO_4)_2]^+$ and $[L_3Mn_2^{III/IV}O_2(ClO_4)_2]^+$, where L = bpy or phen, were used to obtain the kinetics of μ-O exchange. This was because the intact dimeric species $[L_4Mn_2^{III/IV}O_2(ClO_4)_2]^+$ was not observed in the ESI-MS of either complex. As pointed out above, the isotope incorporation in the fragment species does reveal information on the isotope incorporation in the intact species in solution. This is confirmed by the fact that the rates obtained from following either peak are identical within experimental error for both **2** and **3**. Only one value is, therefore, reported for each in Table 1.

Complexes 5, 6. We observed no significant shift in the isotope pattern for **5** over the time that it remains stable in solution (~12 h). **6** seems to be indefinitely stable and shows no significant shift even after several days. Thus, a shift within the experimental error was assumed to occur to obtain an upper limit of the exchange rate for both these compounds. Complexes **5** and **6** contain five and six potentially exchangeable μ-oxos, respectively. To obtain observed rate constants, k_{obs}, for these compounds, it is tedious and unnecessary to obtain the expressions for all exchange intermediates (unexchanged, singly exchanged, and so on, up to completely exchanged). The expression for the unexchanged species suffices to yield k_{obs}, as explained above for **1** to **4**^{ox}.

Comparison of Rates: Factors Affecting Ligand Exchange. An examination of the values listed in Table 1 shows several factors that affect exchange rates. These are discussed below.

Oxidation State of Metal Center. High-spin octahedral Mn^{III} (d^4) is a Jahn−Teller distorted ion, whereas octahedral Mn^{IV} is a relatively nonlabile d^3 ion. The presence of labile Mn^{III} drastically increases μ-O ligand exchange rates, as is evident from a comparison of the present series of complexes. Complexes **5** and **6**, containing only Mn^{IV} ions, show μ-O exchange rates that are several orders of magnitude slower than those of the mixed-valent compounds studied here. The $Mn_2^{IV/IV}$ dimer **4**^{ox}, while still significantly slower than the corresponding $Mn_2^{III/IV}$ dimer **4**, undergoes μ-O exchange much faster than **5** and **6**. While **4**^{ox} is not directly comparable to **5** or **6** due to differences in core structures and identity of ligands, the unavoidable presence of **4** in the solution of **4**^{ox} could potentially enhance the observed exchange rates for **4**^{ox} (as discussed above). However, the differences in μ-O exchange rates measured in this study agree well with theoretical estimates of the change in ligand exchange rates with a change in oxidation state of Mn from +3 to +4.[47]

The solution of **5** also contains small amounts of a $Mn_2^{III/IV}$ species.[34] However, interconversion between **5** and the $Mn_2^{III/IV}$ species is expected to be much slower than the simple electron transfer and bond-length adjustment process leading to interconversion between **4** and **4**^{ox}. Therefore, the presence of $Mn_2^{III/IV}$ in the solution of **5** is expected to have a relatively small effect on the observed μ-O ligand exchange rate for **5**. We conclude that μ-O ligand exchange on a Mn center, which remains in the +4 oxidation state, will be one or more orders of magnitude slower than on a Mn^{III} center or on a Mn center that can switch between +4 and +3 states during the time of exchange.

Presence of Labile Coordination Site on Metal. The complexes **1** and **2**, in addition to having the same metal oxidation state and core structure, also have very similar stereoelectronic properties of the chelating ligands around Mn. However, the μ-O exchange rate for **1** is ~5 times faster than for **2**. The most significant difference between **1** and **2**, which could lead to increased lability in **1**, is the presence of one labile terminal coordination site on each Mn in **1** (occupied by coordinated waters in the solid state). Thus, the presence of a labile terminal water-binding site leads to enhancement of μ-O exchange rates.

Lability of Chelating Ligands. Complexes **2** and **3**, while very similar, are expected to differ in the ease of de-coordination of the chelating ligands. While bpy can undergo sequential de-coordination of the pyridine rings by rotation along the interring single bond, phen must de-coordinate both rings simultaneously, due to the planar bridge between two pyridine rings. This was suggested to be a determining factor for the significantly different rates of the cluster expansion reactions of **2** and **3** by Manchanda et al.[48] However, the μ-O exchange rates of the two complexes are essentially the same. This indicates that de-coordination of chelating ligands, if at all required, is not a rate-determining step in the μ-O exchange process.

Identity of Exchangeable Ligand. The exchange of μ-O with free H_2O requires rearrangement of the Mn_2O_2 core during the breakage of a Mn−μ-O bond and also involves the double deprotonation of a water molecule. The OAc^- exchange, on the other hand, could proceed by elementary ligand substitution steps. Moreover, the bonds between the strongly donating O^{2-} groups and Mn are expected to be stronger than those between Mn and OAc^-. In keeping with the above considerations, μ-O exchange was found to be ~120 times slower than μ-OAc exchange for **4**. A similar comparison for **4**^{ox} is complicated due to the presence of **4** in a solution of **4**^{ox}.

Summary and Conclusions

Wydrzynski and co-workers have examined in detail the incorporation of oxygen atoms from bulk water into the evolved

(47) Lundberg, M.; Blomberg, M. R. A.; Siegbahn, P. E. M. *Theor. Chem. Acc.* **2003**, *110*, 130−143.
(48) Manchanda, R.; Brudvig, G. W.; Crabtree, R. H. *New J. Chem.* **1994**, *18*, 561−568.

dioxygen in the OEC of PSII.[17−21] Because of their experimental design, the rate of incorporation reflects the rate at which bulk water incorporates into the water-binding site of the OEC in a given S state. The following points emerge from their study: (a) The two substrate water molecules bind to separate sites throughout the S-state cycle. (b) The two sites are characterized by very different exchange rates. The slow exchanging site exchanges ∼10 times slower than the fast exchanging site in the S_3 state, ∼100 times slower in the S_2 state, and ≥5000 times slower in the S_1 state. (c) The two substrate waters are already bound to the OEC at the S_2 state. (d) Ca^{2+} is involved in substrate water binding at the slow exchanging site. (e) The rate constants measured at 10 °C for the slow exchanging site range from 2.2×10^{-2} s^{-1} in the S_1 state to 14 s^{-1} in the S_0 state, and those for the fast exchanging site range from 30 s^{-1} in the S_3 state to ≥100 s^{-1} in the S_1 and S_2 states.

It is generally accepted that the redox active Mn in the S_2 state of the OEC are in the +3 and +4 oxidation states with di-μ-O linkages. Complex **1**, a di-μ-O $Mn_2^{III/IV}$ dimer with water binding sites, can therefore be considered a model for the S_2 state. The μ-O exchange rate in **1** is $\sim 5 \times 10^4$ times slower than the fast rate of exchange detected in the S_2 state. In the present experiments, $[H_2{}^{18}O] = 0.26$ M, whereas $[H_2{}^{18}O] =$ 7.4 M in the experiments by Wydrzynski et al. This ∼30-fold difference in $[H_2{}^{18}O]$ would translate into a smaller difference in effective concentrations of $H_2{}^{18}O$, considering that water access to the OEC is expected to be greatly restricted in comparison to a small molecule in solution. The difference in $[H_2{}^{18}O]$ is therefore unlikely to account for the observed difference in exchange rates between the model complex **1** and the S_2 state OEC. While the factors affecting ligand exchange rates may be quite complex in a protein environment[47] and there are differences in the experimental procedures for determination of the rates of exchange in the OEC and Mn model complexes, we conclude that the fast exchange rate in the S_2 state is too fast to be attributed to water incorporation into a μ-O site on Mn.

There has been considerable debate on the site of oxidation during the S_2 to S_3 transition,[16,49] with some authors favoring Mn oxidation and others favoring oxidation of a ligand to the OEC. According to the former view, μ-O ligand exchange rates on Mn should slow considerably upon going from the S_2 to the S_3 state, with the OEC most likely changing from a $Mn^{III}Mn_3^{IV}$ state to a Mn_4^{IV} state. Predicting the effect of ligand-centered oxidation, on the other hand, is more complicated. If oxidation of a μ-O ligand occurs, then μ-O exchange rates are expected to be affected, but the direction or magnitude of this effect cannot be predicted due to the absence of exchange studies on Mn model systems with μ-O• radicals. If a different ligand, such as the redox active tyrosine or histidine, is oxidized, μ-O exchange rates are unlikely to be affected significantly. In any case, the fast exchange rate of 30 s^{-1} observed in the S_3 state is $\sim 1 \times 10^4$ times greater than that observed for the μ-O ligands in **1** and is unlikely to reflect water exchange with a μ-O site on Mn.

The slow rate of exchange measured at 20 °C in the OEC[50] approaches the μ-O exchange rate for **1** somewhat more closely, being ∼25 times faster in the S_1 state, ∼1800 times faster in the S_2 and S_3 states, and ∼5600 times faster in the S_0 state. While the substantially faster exchange in the S_0 state is consistent with the unlikeliness of a substrate water being doubly deprotonated to a μ-O bridge by such an early S state, the rate in the S_1 state is more consistent with the expected rate of μ-O exchange. We also note that the experimental activation energies of the slow exchange in the S_1 to S_3 states are ∼75 kJ mol^{-1}, in reasonably good agreement with the theoretically calculated value[47] of ∼80 kJ mol^{-1}.

We note that the exchange rates of bridging oxo and hydroxo ligands measured in complexes of other metals span a wide range,[51] as do the rates measured in this study. A useful comparison between the two is difficult due to the simultaneous variation of structure, formal charge, number of electrons, etc. An example of the measurement of a μ-O exchange rate in a protein is the 8×10^{-4} s^{-1} rate attributed to a μ-O ligand on Fe^{III} in ribonucleotide reductase,[52] although there is no obvious comparison to the exchange rates in the OEC.

In summary, we have measured the rates of ligand exchange in several high-valent multinuclear oxomanganese complexes. Our method demonstrates the use of ESI-MS to measure the rates of isotope exchange reactions in general. We show that the exchange rates are sensitive to the structure and oxidation state of the complex. Although exchange rates in a protein may be governed by many complex factors, the nature of the dependences in model complexes provides a basis for the interpretation of the changes in rates of isotope exchange with changes in the S states of the OEC. On this basis, we conclude that both substrate waters do not bind as μ-O bridges between Mn atoms in the S_2 and S_3 states of the OEC, thus providing additional constraints on proposed mechanisms of water oxidation by the OEC. However, μ-O exchange rates are likely to be affected by hydrogen bonding, ligation to other metal centers such as the Ca^{2+} cofactor in the OEC, and the specific pathway of exchange. These are presently under investigation.

Acknowledgment. This work has been supported by the National Institutes of Health (GM32715).

Supporting Information Available: ESI-MS and peak assignments of complexes **2**, **3**, and **4**. This material is available free of charge via the Internet at http://pubs.acs.org.

JA061348I

(49) Limburg, J.; Szalai, V. A.; Brudvig, G. W. *J. Chem. Soc., Dalton Trans.* **1999**, *9*, 1353−1362.
(50) Hillier, W.; Wydrzynski, T. *Phys. Chem. Chem. Phys.* **2004**, *6*, 4882−4889.
(51) Hillier, W.; Wydrzynski, T. *Biochim. Biophys. Acta* **2001**, *1503*, 197−209.
(52) Sjöberg, B.-M.; Loehr, T. M.; Sander-Loehr, J. *Biochemistry* **1982**, *21*, 96−102.